Magn Reson Med Sci 2021; 20; 325–337
doi:10.2463/mrms.mp.2020-0044
Published Online: October 16, 2020

MAJOR PAPER

Synthetic MRI with T_2-based Water Suppression to Reduce Hyperintense Artifacts due to CSF–Partial Volume Effects in the Brain

Tokunori Kimura*, Kousuke Yamashita, and Kouta Fukatsu

Purpose: Our purpose was to assess our proposed new synthetic MRI (synMRI) technique, combined with T_2-based water suppression (T_2wsup), to reduce cerebral spinal fluid (CSF)–partial volume effects (PVEs). These PVEs are problematic in the T_2-weighted fluid-attenuation inversion recovery (FLAIR) images obtained by conventional synMRI techniques.

Methods: Our T_2wsup was achieved by subtracting additionally acquired long TE spin echo (SE) images of water signals dominant from the originally acquired images after T_2 decay correction and a masking on the long TE image using the water volume (V_w) map to preserve tissue SNR, followed by quantitative mapping and then calculation of the synthetic images. A simulation study based on a two-compartment model including tissue and water in a voxel and a volunteer MR study were performed to assess our proposed method. Parameters of long TE and a threshold value in the masking were assessed and optimized experimentally. Quantitative parameter maps of standard and with T_2wsup were generated, then wsup-synthetic FLAIR and SE images were calculated using those suitable combinations and compared.

Results: Our simulation clarified that the CSF–PVE artifacts in the standard synthetic FLAIR increase T_2 as the water volume increases in a voxel, and the volunteer MR brain study demonstrated that the hyperintense artifacts on synthetic images were reduced to < 10% of V_w in those with the standard synMRI while keeping the tissue SNR by selecting optimal masking parameters on additional long TE images of TE = 300 ms. In addition, the wsup-synthetic SE provided better gray-white matter contrasts compared with the wsup-synthetic FLAIR while keeping CSF suppression.

Conclusion: Our proposed T_2wsup-synMRI technique makes it easy to reduce the CSF–PVE artifacts problematic in the synthetic FLAIR images using the current synMRI technique by adding long TE images and simple processing. Although further optimizations in data acquisition and processing techniques are required before actual clinical use, we expect our technique to become clinically useful.

Keywords: *synthetic magnetic resonance imaging, fluid-attenuation inversion recovery, partial volume effects, hyperintense artifacts, signal-to-noise ratio*

Introduction

Synthetic MRI (synMRI) generates several kinds of contrast-weighted images by synthesizing quantitative parameter maps of proton density (PD), longitudinal relaxation time (T_1), and transverse relaxation time (T_2) obtained using acquired fast-spin echo (FSE) data. The synMRI is beginning to be used clinically because of the advantages of saving total examination time and the freedom to select MRI acquisition parameters of TR, TI, and TE. Also, using synMRI, quantitative parameter maps can be obtained.[1–7] However, synthetic T_2-weighted images (T_2WIs) of fluid-attenuation inversion recovery (FLAIR) or a double-inversion recovery (DIR) introduces hyperintense artifacts at the border zone of tissue and ventricle or the surface of the brain cortex. This is thought to be caused by partial volume effects (PVE) introduced by including brain tissue and cerebral spinal fluid (CSF) in a single voxel.[3–6] Nevertheless, there is a quantitative relationship between the CSF–PVE and the hyperintense artifacts between the standard synthetic FLAIR

Department of Radiological Science, Shizuoka College of Medicalcare Science, Hamamatsu, Shizuoka, Japan

*Corresponding author: Department of Radiological Science, Shizuoka College of Medicalcare Science, 2000, Hirakuchi, Hamakita-ku, Hamamatsu, Shizuoka 434-0041, Japan. Phone: +81-053-585-1551, E-mail: enocolo.tk@gmail.com

Received: March 12, 2020 | Accepted: August 22, 2020

(std-synFLAIR) image, and therefore fundamental solutions have not been clarified yet. FLAIR, including DIR imaging, is very important for clinical MR brain imaging to separate lesions from CSF; however, it requires a relatively long acquisition time. Therefore, the first priority is to solve the problem of CSF–PVE artifacts in synthetic FLAIR images with a minimum time load, in order to further encourage this technique in clinical use.

The longitudinal magnetization (Mz) of water in the acquired FLAIR is ideally zero; however, the quantitative maps of T_1, T_2, and PD obtained by the std-synMRI are calculated from the mixed signals of tissue and water. Therefore, the T_2 decay behavior differs depending on the rate of water in a voxel between the acquired FLAIR and std-synFLAIR images. It is thought that those T_2 differences introduce the CSF–PVE hyperintense artifacts in the std-synFLAIR image, and this problem is not easily solved unless tissue and water components in each voxel can be separated.

This study was done to quantitatively clarify the cause of CSF–PVE-dependent hyperintense artifacts and then to assess a new synMRI technique to reduce those artifacts, especially in FLAIR, without loss of the tissue SNR. The new technique combines synMRI and a T_2-based water suppression technique (T_2wsup). The assessment was done using a simulation and MR volunteer studies.

Materials and Methods

Model

As shown in Fig. 1, when a unit voxel of volume V consists of two-components of water and tissue, the MR signal in the voxel is based on a two-compartment model of water volume V_w, tissue volume V_t, and the voxel volume is

$$V = V_w + V_t = 1 \tag{1}$$

and the voxel mean proton density is

$$\mathrm{PD} = V_w \cdot \mathrm{PD}_w + V_t \cdot \mathrm{PD}_t \tag{2}$$

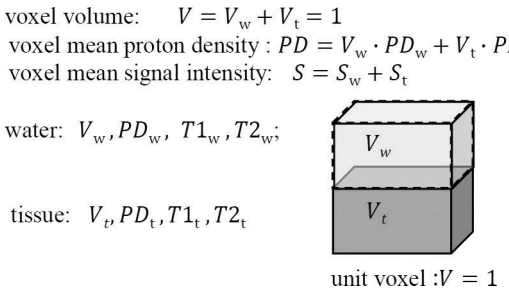

Fig. 1 A two-compartment voxel model for containing water and tissue components in a single voxel. PD, proton density; T_1, longitudinal relaxation time; T_2, transverse relaxation time.

Likewise, the suffix w and t denote, respectively, the parameters for water and for tissue.

Signal intensities (SIs) of spin echo (SE) and inversion recovery (IR)-SE for a two-compartment model are, respectively,

$$S_{\mathrm{SE}}(\mathrm{TR}, \mathrm{TE}, \mathrm{PD}, \mathrm{T}_1, \mathrm{T}_2) = S_{\mathrm{SEw}}(\mathrm{TR}, \mathrm{TE}, \mathrm{PD}_w, \mathrm{T}_{1w}, \mathrm{T}_{2w}) + S_{\mathrm{SEt}}(\mathrm{TR}, \mathrm{TE}, \mathrm{PD}_t, \mathrm{T}_{1t}, \mathrm{T}_{2t}) \tag{3}$$

and

$$S_{\mathrm{IR}}(\mathrm{TR}, \mathrm{TE}, \mathrm{PD}, \mathrm{T}_1, \mathrm{T}_2) = S_{\mathrm{IRw}}(\mathrm{TR}, \mathrm{TI}, \mathrm{TE}, \mathrm{PD}_w, \mathrm{T}_{1w}, \mathrm{T}_{2w}) + S_{\mathrm{IRt}}(\mathrm{TR}, \mathrm{TI}, \mathrm{TE}, \mathrm{PD}_t, \mathrm{T}_{1t}, \mathrm{T}_{2t}) \tag{4}$$

where

$$S_{\mathrm{SEw,t}}(\mathrm{TR}, \mathrm{TE}, \mathrm{PD}_{w,t}, \mathrm{T}_{1w,t}, \mathrm{T}_{2w,t}) = \mathrm{PD}_{w,t} \cdot \mathrm{DecayT}_{1\mathrm{SEw,t}}(\mathrm{TR}, \mathrm{T}_{1w,t}) \cdot \mathrm{DecayT}_{2w,t}(\mathrm{TE}, \mathrm{T}_{2w,t}) \tag{5}$$

$$S_{\mathrm{IRw,t}}(\mathrm{TR}, \mathrm{TI}, \mathrm{TE}, \mathrm{PD}_{w,t}, \mathrm{T}_{1w,t}, \mathrm{T}_{2w,t}) = \mathrm{PD}_{w,t} \cdot \mathrm{DecayT}_{1\mathrm{IRw,t}}(\mathrm{TR}, \mathrm{TI}, \mathrm{T}_{1w,t}) \cdot \mathrm{DecayT}_{2w,t}(\mathrm{TE}, \mathrm{T}_{2w,t}) \tag{6}$$

$$\mathrm{DecayT}_{1\mathrm{SEw,t}}(\mathrm{TR}, \mathrm{T}_{1w,t}) = \left\{1 - 2 \cdot \exp\left(-\frac{\mathrm{TR} - \frac{\mathrm{TE}}{2}}{\mathrm{T}_{1w,t}}\right) + \exp\left(-\frac{\mathrm{TR}}{\mathrm{T}_{1w,t}}\right)\right\} \tag{7}$$

$$\mathrm{DecayT}_{1\mathrm{IRw,t}}(\mathrm{TR}, \mathrm{TI}, \mathrm{T}_{1w,t}) = \left\{1 - 2 \cdot \exp\left(-\frac{\mathrm{TI}}{\mathrm{T}_{1w,t}}\right) + 2 \cdot \exp\left(-\frac{\mathrm{TR} - \frac{\mathrm{TE}}{2}}{\mathrm{T}_{1w,t}}\right) - \exp\left(-\frac{\mathrm{TR}}{\mathrm{T}_{1w,t}}\right)\right\} \tag{8}$$

$$\mathrm{DecayT}_{2w,t} = \exp\left(-\frac{\mathrm{TE}}{\mathrm{T}_{2w,t}}\right) \tag{9}$$

When analyzing in the std-synMRI based on the single-compartment model shown in Eq. (5) or Eq. (6) without suffix w or t, the averaged voxel values are used for calculating those quantitative parameters, resulting in parameters that become close to the water values with increasing V_w. In contrast, if water suppression (wsup) is perfectly achieved, Eqs. (3) and (4) become respectively as

$$S_{\mathrm{SE}}(\mathrm{TR}, \mathrm{TE}, \mathrm{PD}, \mathrm{T}_1, \mathrm{T}_2) = S_{\mathrm{SEt}}(\mathrm{TR}, \mathrm{TE}, \mathrm{PD}_t, \mathrm{T}_{1t}, \mathrm{T}_{2t}) \tag{3′}$$

and

$$S_{\mathrm{IR}}(\mathrm{TR}, \mathrm{TE}, \mathrm{PD}, \mathrm{T}_1, \mathrm{T}_2) = S_{\mathrm{IRt}}(\mathrm{TR}, \mathrm{TI}, \mathrm{TE}, \mathrm{PD}_t, \mathrm{T}_{1t}, \mathrm{T}_{2t}) \tag{4′}$$

These mean that the quantitative parameters of tissue can be obtained even analyzing based on a single-compartment model when using wsup data.

Data acquisition and processing flow

Our proposed water suppression (wsup) technique is based on the T_2 difference between tissue and water, similar to the high-intensity REduction (HIRE) technique,[8] where the additionally acquired long TE image of the dominant water signal is subtracted from the acquired standard TE image. In our method, the water suppressed quantitative maps are calculated using these wsup images, and finally synthetic images with arbitrary combinations of acquisition parameter maps are obtained. A general processing flow for our proposed technique of wsup-synMRI and the example of using minimum number of data is shown in Fig. 2. The basic idea is that the wsup for the acquired images is performed before calculating quantitative parameters, then followed by calculating quantitative parameter maps and synthetic images. In this, a key flow is wsup for acquired images, as shown in Fig. 3.

Acquired image data at the generalized condition are $S_{acq}(TE_m, r)$, $TE_1 < TE_2$ ---< TE_M, and water image is $S_{acq}(TE_{long}, r)$, $TE_{long} = TE_M$, where r denotes the spatial position of each image in all imaging space, R. Below, our proposed technique is explained in 3 steps.

Water suppression for acquired images

a. First, a water volume ratio map, $V_w(r)$ $(0 \le V_w(r) \le 1)$ is obtained, normalizing by dividing the pure water (CSF) SI of the long TE image, $S_{acq}(TE_{long}, r)$. The easiest way to normalize is to use a maximum value of the long TE image as

$$S_{acq.max}\left(TE_{long}\right) = \max_{r \in R}\left[S_{acq}\left(TE_{long}, r\right)\right] \tag{10}$$

$$V_w(r) = \frac{S_{acq}\left(TE_{long}, r\right)}{S_{acq.max}\left(TE_{long}\right)} \tag{11}$$

where $\underset{r \in R}{\text{Max}}[\ ]$ is an operator to obtain maximum value of [ ] for all r defined in R.

Optionally, it is possible to make robust by enlarging the pure CSF portion as

$$V_w(r) = 1 : S_{acq}(TE_{long}, r) \ge Th V_{wmax} \cdot S_{acq.max}(TE_{long}); \\ = \frac{S_{acq}(TE_{long}, r)}{Th V_{wmax} \cdot S_{acq.max}(TE_{long})} : \text{ otherwise} \tag{11'}$$

where the $Th V_{wmax}$ is a threshold to include pure CSF portions with a margin by setting $Th V_{wmax} < 1$. If $Th V_{wmax} = 1$ in Eq. (11′), then Eq. (11′) becomes Eq. (11).

b. Second, a scaling for T_2 decay correction, $\alpha(TE_m)$, is obtained by using T_2 of pure water, T_{2w}, as

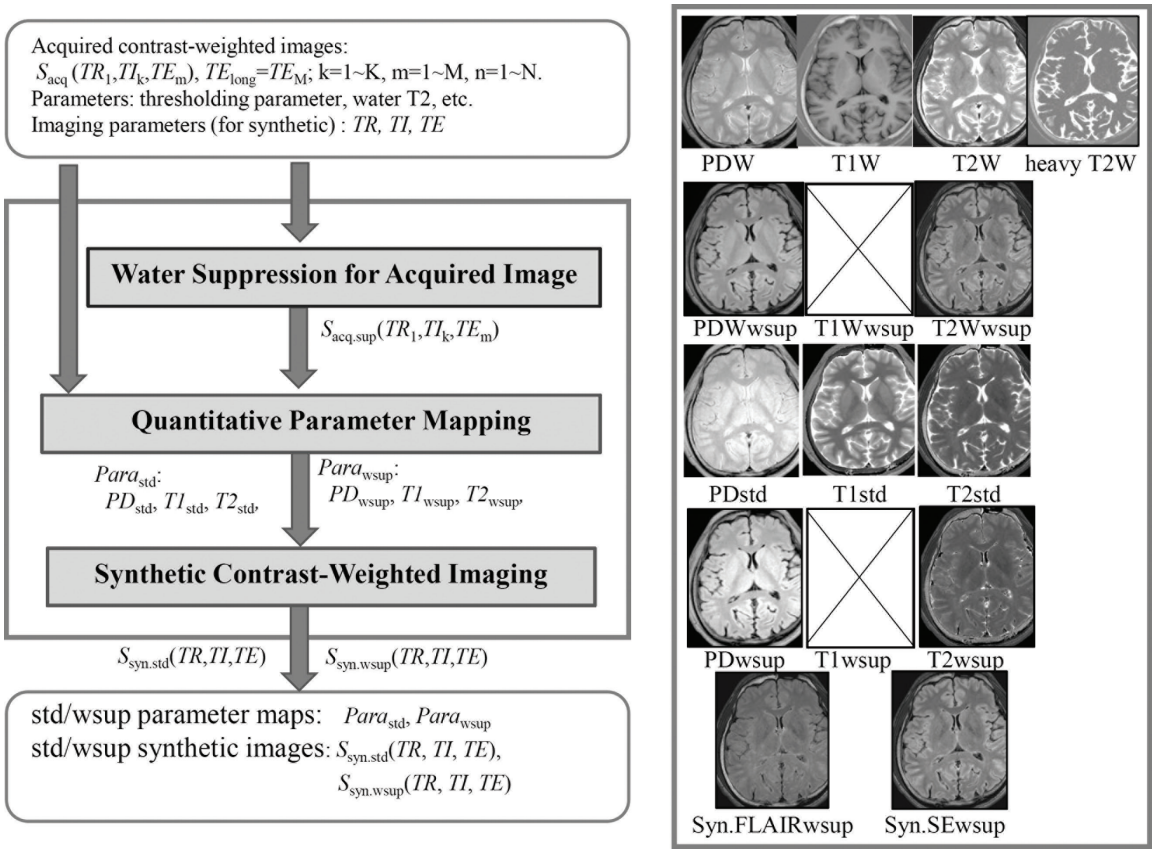

Fig. 2 General whole process flow for our proposed technique of T_2wsup-synMRI. On the right are example images of each stage using minimum number (L = 1, M = 3) of acquired images when T_1wsup is not required. T_2wsup-synMRI, T_2-based water-suppressed synthetic MRI.

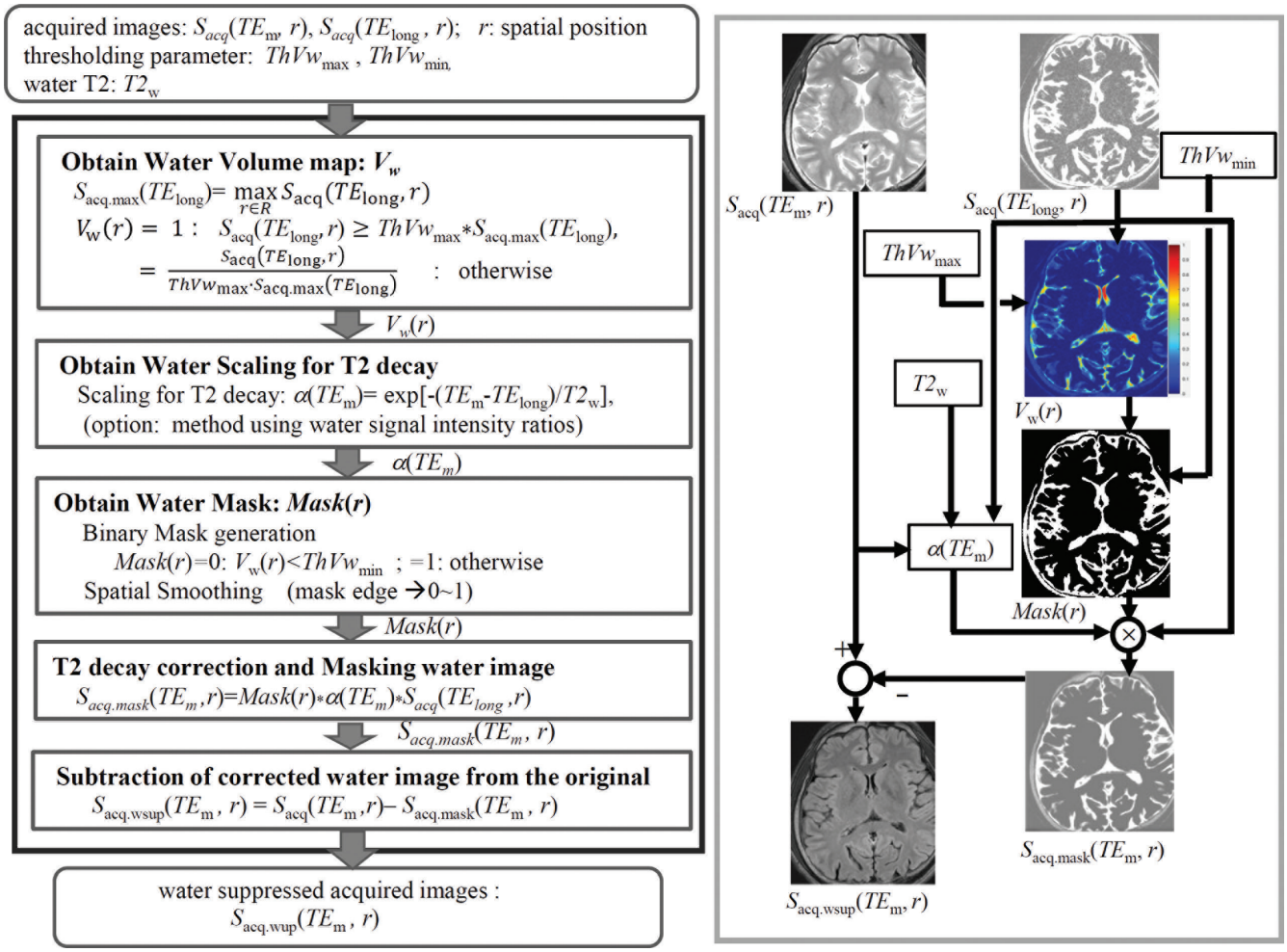

Fig. 3 Detailed process flow for water suppression for acquired images in Fig. 2, where the representative flow is shown. The details are given in the main text.

$$\alpha(\mathrm{TE}_m) = \exp\left[-\frac{\left(\mathrm{TE}_m - \mathrm{TE}_{\mathrm{long}}\right)}{\mathrm{T}_{2\mathrm{w}}}\right],\ m = 1, 2, -, M-1 \quad (12)$$

Or, when the T_{2w} is unknown, the ratio of the averaged SI within the same pure water regions among different TEs is

$$\alpha(\mathrm{TE}_m) = \frac{S_{\mathrm{acq.mean}}(\mathrm{TE}_m)}{S_{\mathrm{acq.mean}}(\mathrm{TE}_{\mathrm{long}})}. \quad (12')$$

where

$$S_{\mathrm{acq.mean}}(\mathrm{TE}_{\mathrm{m,long}}) = \underset{r' \in V_w(r)=1}{\mathrm{Mean}}\left[S_{\mathrm{acq}}(\mathrm{TE}_{\mathrm{m,long}}, r)\right] \quad (13)$$

$\underset{r \in V_w(r)=1}{\mathrm{Mean}}[\ ]$ is an operator to obtain averaged value of [ ] for all r satisfying $r \in V_w(r) = 1$

c. Third, a spatial mask, $\mathrm{Mask}(r)$ to keep tissue SNR after subtraction is obtained as

$$\mathrm{Mask}(r) = 1 : V_w(r) > \mathrm{Th}V_{w\min}; = 0 : \text{otherwise} \quad (14)$$

where $\mathrm{Th}V_{w\min}$ is a threshold value (0–1) when pure (100%) water is 1, decided experimentally dependent on $\mathrm{TE}_{\mathrm{long}}$ but it can be commonly used once it is decided. Then, a spatial smoothing filter is applied to the $\mathrm{Mask}(r)$ to smooth the boundary of 0 and 1 in the mask.

d. Fourth, the water images after T_2 decay correction and masking, $S_{\mathrm{acq.mask}}(\mathrm{TE}_m, r)$, are obtained from the corresponding standard acquired images with the same condition as

$$S_{\mathrm{acq.mask}}(\mathrm{TE}_m, r) = \mathrm{Mask}(r) \cdot \alpha(\mathrm{TE}_m) \cdot S_{\mathrm{acq.mask}}(\mathrm{TE}_{\mathrm{long}}, r) \quad (15)$$

e. Finally, water-suppressed acquired images, $S_{\mathrm{acp.wsup}}(\mathrm{TE}_m, r)$, are obtained by subtracting the corrected water images from the originally acquired images of the same TE as

$$S_{\mathrm{acq.wsup}}(\mathrm{TE}_m, r) = S_{\mathrm{acq}}(\mathrm{TE}_m, r) - S_{\mathrm{acq.mask}}(\mathrm{TE}_m, r) \quad (16)$$

Quantitative parameter mapping

After obtaining those wsup images for acquired images, quantitative maps are calculated using those wsup images in addition to the standard images. When multiple images (data points) along TE or TI are acquired, unknown quantitative parameters for wsup: $Para_{wsup} = (T_{2wsup}, T_{1wsup}, PD_{wsup})$ $\{\sim (T_{2t}, T_{1t}, PD_t)\}$, and for standard: $Para_{std} = (T_{2std}, T_{1std}, PD_{std})$, can be respectively calculated using acquired images of wsup ($S_{acq.wsup}$) and standard (S_{acq}) by least squares method based on the single-compartment model equations in Eq. (5) or Eq. (6).

The quantitative parameters can also be obtained using the minimum number (4 or 5) of the acquired images of wsup and standard, as shown in Table 1, based on the following simple equations as

$$T_2 = \frac{TE_2 - TE_1}{\ln\left\{\frac{S_{SE}(TR_1, TE_1)}{S_{SE}(TR_1, TE_2)}\right\}} \quad (17)$$

$$T_1 = -\frac{TI_1}{\ln\left[\frac{\left\{1 - \frac{S_{IR}(TR_1, TI_1, TE_1)}{S_{SE}(TR_1, TE_1)}\right\}}{2}\right]} \quad (18)$$

$$PD = \frac{S_{SE}(TR_1, TE_1)}{DecayT_{1IR}(TR_1, TI_1, T_1) \cdot DecayT_2(TE_1, T_2)} \quad (19)$$

Table 1 Simulation conditions of quantitative parameters and imaging parameters

Parameters	#	Water (CSF)	Tissue
Quantitative[a]			
PD		0.97	0.8
T_1 [ms]		4000	1000
T_2 [ms]		1910	100
Imaging[b]			
	1	S_{SE} (TR_1,TE_1)	
	2	S_{SE} (TR_1,TE_2)	
Acquired data	3	S_{SE} (TR_1,TE_3)	
	4	S_{IR} (TR_1,TI_1,TE_1)	
	5	S_{IR} (TR_1,TI_1,TE_3)	
TR_1 [ms]		10000	
TE_1,TE_2, TE_3 [ms]		20, 100, 500	
TI_1 [ms]		1000	
Synthetic			
TR [ms]		10000	
TE [ms]		20	
TI [ms] (for FLAIR)		2350	

[a]Quantitative parameters were referred to Warntjes et al.[1] [b]TE_3 correspond to TE_{long}. CSF, cerebral spinal fluid; FLAIR, fluid-attenuation inversion recovery; TE, echo time.

where the MR parameters of TR, TI, and TE are selected as $TR_1 > T_{1w} > T_{1t}$, $TI_1 \sim T_{1t}$, and $TE_2 > TE_1$ to be close to the correct values. Here, if the TE_1 is selected to be shortest, the PD_{wsup} can be obtained using T_{1std} because of $DecayT_{1IR}(TR_1, TI_1, T_1) \sim 1$. When the T_{1wsup} image is required, another long TE image (#5 in Table 1) must be acquired, but it is not necessary for calculating the wsup-synthetic images of FLAIR and SE.

Synthetic contrast-weighted imaging

Synthetic images, both of the standard and wsup, are calculated based on the signal models in Eq. (5) for SE and Eq. (6) for FLAIR, respectively, by the following 3 parameter combinations: std-synFLAIR/SE: (PD_{std}, T_{1std}, T_{2std}), wsup-synFLAIR: (PD_{std}, T_{1std}, T_{2wsup}), and wsup-synSE: (PD_{wsup}, T_{1std}, T_{2wsup}). Here, the parameter combination for the wsup-synFLAIR is selected to be equivalent to the acquired FLAIR contrast, and that for the wsup-synSE is selected to provide a new wsup contrast, enabling tissue SNR without inversion.

Simulation

First, to compare the degree of PVE quantitatively for the standard and proposed wsup methods, the quantitative parameters of PD, T_1, and T_2 based on the single-compartment model were calculated as a parameter of a water volume fraction, V_w. The parameters in this simulation are summarized in Table 1. Voxel mean values of quantitative parameters were calculated from those averaged SIs as a parameter of V_w and with a parameter of subtracting weight α(TE) for ideal and those scaled versions with 0.8 and 0.9.

Second, the synFLAIR and synSE SIs for the standard and wsup were calculated as a function of TE, each with a parameter of V_w.

MRI experiments

In the MR experiments, the first 4 data points in Fig. 2 were acquired for our proposed synMRI. A healthy volunteer study was performed on an MRI machine (Galan 3T [ZGO]; Canon Medical Systems, Tochigi, Japan) with a 32-channel head coil after obtaining informed consent. An FSE sequence was used, and the acquisition parameters were the following: parallel imaging (SPEEDER; Canon Medical Systems) of speed-up factor 2; acquisition matrix of 256 × 256; display matrix of 512 × 512 after sinc interpolation; FOV = 23 cm; slice thickness = 5 mm; number of slices was commonly selected at maximum for TE_{long} = 500 ms; number of average, 1; TR_1 = 10,000 ms, TE_1 = 20 ms, TE_2 = 100 ms, TE_{long} = 300 or 500 ms, TI_1 = 1000 ms, where each different contrast data were acquired with the separated sequence. An adiabatic inversion pulse was used for IR to reduce RF field (B1) inhomogeneity. The scaling factor of α(TE) obtained with the SI ratio of $ThV_{wmax} = 1$, which corresponds to fitted water T_2 of T_{2w} = 990 ms, was used for T_2 decay correction of the water SI of each TE. The acquired FLAIR with a coverage interleaved multi-slice was used for comparison. This is introduced to improve both the inversion efficiency and CSF

in-flow artifacts by setting the inversion thickness as nearly twice the standard; however, the acquisition time requires 2 times the standard.

For assessments, masking effects as a parameter of ThV_{wmin} and the difference of TE for long TE images were compared, then the optimal parameters were used for the following steps. Quantitative maps and synthetic images of FLAIR and SE each with the standard and wsup were compared as a parameter of TE, and then the acquired FLAIR and wsup-synthetic images of FLAIR and SE were also compared.

Results

Simulation

The quantitative parameters for the water-suppressed (wsup) data, compared with the standard (w/o wsup) data, became close to those for the tissue components when the water signals were ideally suppressed. The wsup effects were weaker when decreasing the subtracting weight, α(TE), from the ideal (Fig. 4).

For the SIs as a function of TE (Fig. 5), the hyperintense signals in std-synFLAIR were because the averaged T_2 values in a voxel increased as the water volume, V_w, increased, and those effects were stronger with increasing TE. However, those effects were reduced in our proposed wsup-synFLAIR. Furthermore, our proposed wsup-synSE provided SNR improvements by 10–20% in this condition in addition to CSF suppression, because the tissue signals were not IR signals but SE signals. Although this simulation was performed without noise, when considering a noise propagation in actual synMRI, the noise for SE is smaller than the IR-SE due to the smaller contribution of T_1 in SE compared to that in IR-SE.

MR experiments

The effects of water masking against ThV_{wmin} are shown in Fig. 6. The CSF signals were comparably suppressed without loss of tissue SNR by using the wsup-images with masking compared with those without masking. Regarding the relationship with ThV_{wmin}, the tissue SNRs increased as the ThV_{wmin} increased until a certain ThV_{wmin}, while the hyperintensity CSF–PVE artifacts were increased over those ThV_{wmin}. Thus, the optimal ThV_{wmin} was decided considering the trade-off between the tissue SNR and the CSF–PVE artifacts. In our experiments, the optimal ThV_{wmin} values were ThV_{wmin} = 0.10 at TE_{long} = 300 ms and ThV_{wmin} = 0.05 at TE_{long} = 500 ms, and the tissue SNRs were increased by ~80% and ~50% in those conditions, respectively. Comparing the long TE images of TE_{long} = 300 ms with those of TE_{long} = 500 ms, the residual tissue signals of GM and WM were greater for TE_{long} = 300 ms; however, the tissue SNRs of subtracted T_2WI even for TE_{long} = 300 ms were used without subtraction by using the optimal ThV_{wmin}. In this volunteer study, all the wsup images of acquired, quantitative maps, and synthetic images were obtained using the optimal ThV_{wmin} = 0.05 and the long TE image of TE_{long} = 500 ms.

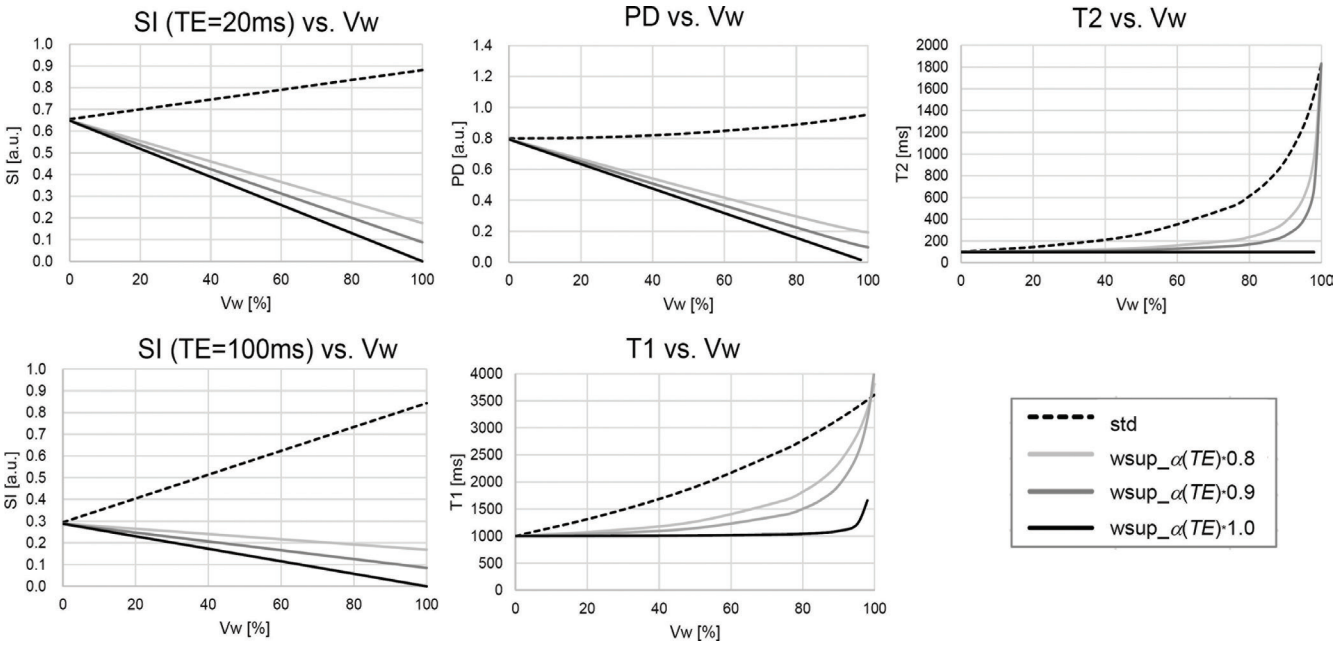

Fig. 4 Simulation results of signal intensities (left) and quantitative parameters (center and right) versus V_w for our T_2-based wsup technique. The standard (std) data became close to water value with increasing V_w but the wsup data showed the values for tissue components by eliminating the water component. The effects of water suppression were weaker as α was smaller, where the T_2 and T_1 for ideal suppression (α * 1) cannot be obtained at V_w = 1 due to zero signal. wsup, water suppression.

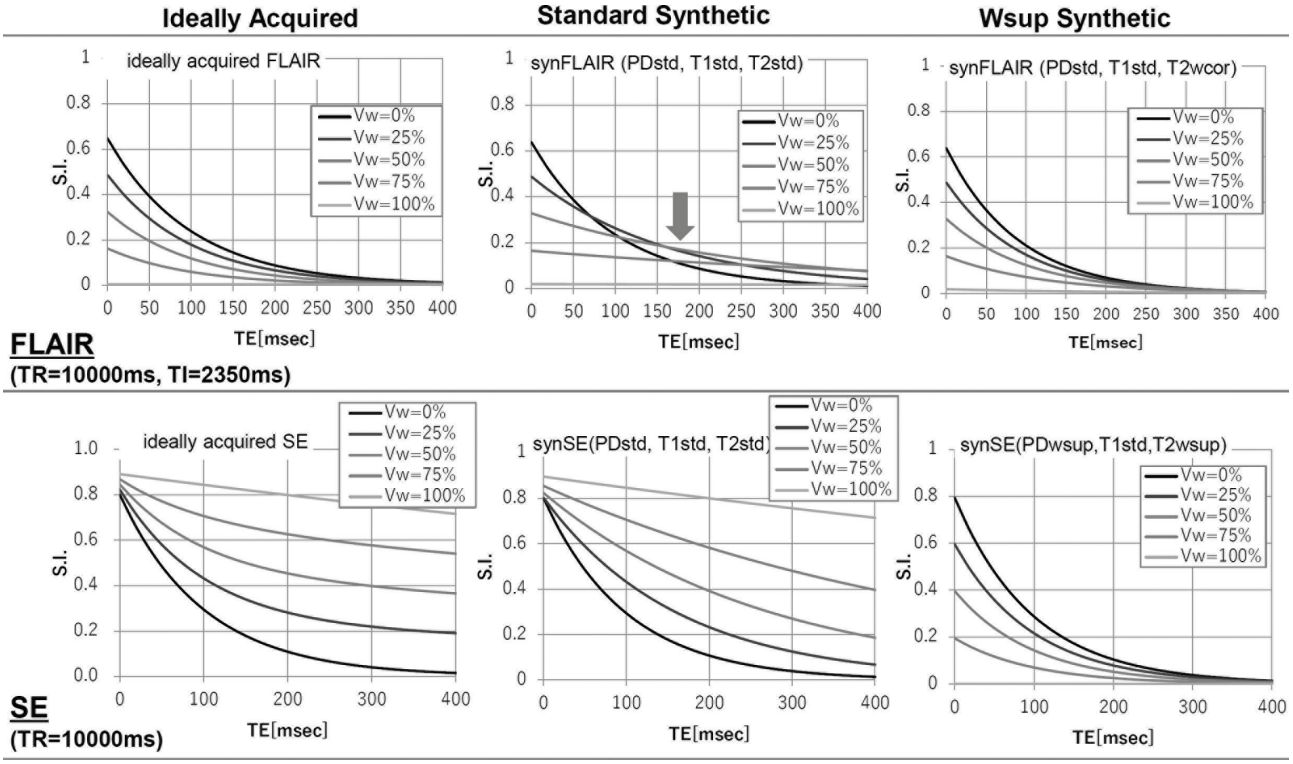

Fig. 5 Simulation results of SIs versus TE with FLAIR (top) and SE (bottom) as parameters of V_w for 3 cases. Note that the SI in standard synthetic-FLAIR increased with increasing TE due to slower T_2 decay with increasing V_w (arrow). These effects were corrected by our proposed wsup-syn technique. Furthermore, the wsup-synSE provided better SNR than the wsup-synFLAIR in addition to CSF suppression, that is, the SIs for wsup-synSE, compared with the wsup-synFLAIR, improved 23%, 17%, and 12%, respectively at V_w = 0%, 25%, 50%. CSF, cerebral spinal fluid; FLAIR, fluid-attenuation inversion recovery; SE, spin echo; SIs, signal intensities; TE, echo time; V_w, water volume; wsup-syn, water suppression synthetic.

Acquired images and quantitative maps for standard and wsup are shown in Fig. 7. The CSF signals in our proposed wsup-images with optimal masking were suppressed compared with those in the standard.

Synthetic images of FLAIR and SE each for standard and wsup as a parameter of TE are shown in Fig. 8. The hyperintense artifacts shown in the std-synFLAIR images, especially at the CSF–PVE portions such as the temporal lobe or cerebellum, were almost reduced in the wsup-synFLAIR images with increasing TE. In addition, the CSF signals in the std-synSE images were perfectly reduced in the wsup-synSE images.

Comparison of the acquired FLAIR images, wsup-synFLAIR, and wsup-synSE is shown in Fig. 9. When comparing the wsup-synFLAIR with the acquired FLAIR images, the tissue contrasts were almost equivalent, while the CSF inflow or motion artifacts shown in the acquired FLAIR image were not introduced in the wsup-synFLAIR images.

Numerical results of acquired are summarized in Table 2 and those quantitative parameters and synthetic images are summarized in Table 3, each with 3 methods of the standard, wsup w/o and with masking, where 2 kinds of TE_{long} were used for wsup. Note that all the tissue SNRs reduced in the wsup w/o masking were perfectly restored by the wsup with masking, comparable to the standard data, and the wsup with masking data using TE_{long} = 300 ms was greatly improved compared with that using TE_{long} = 500 ms.

Discussion

We proposed and assessed a new synthetic MRI technique called T_2wsup-synMRI. This technique was based on a simple T_2-based wsup using additional long TE data to reduce the CSF–PVE artifacts in synthetic FLAIR images obtained by the conventional synthetic MRI technique. We clarified the cause of those artifacts quantitatively with a simulation and then demonstrated that the CSF–PVE artifacts in quantitative maps and synthetic images of FLAIR, as well as SE obtained by our proposed method, were reduced in the MR volunteer study, especially in longer TE for synthetic images.

A limitation of our study was that there were only a few healthy volunteers and a single 3T MRI scanner for the MR study, and the results were processed with the minimum number of acquired data. Below, we discuss our experimental results and the optimization for those parameters, the modification of our proposed technique, alternative techniques, and the future.

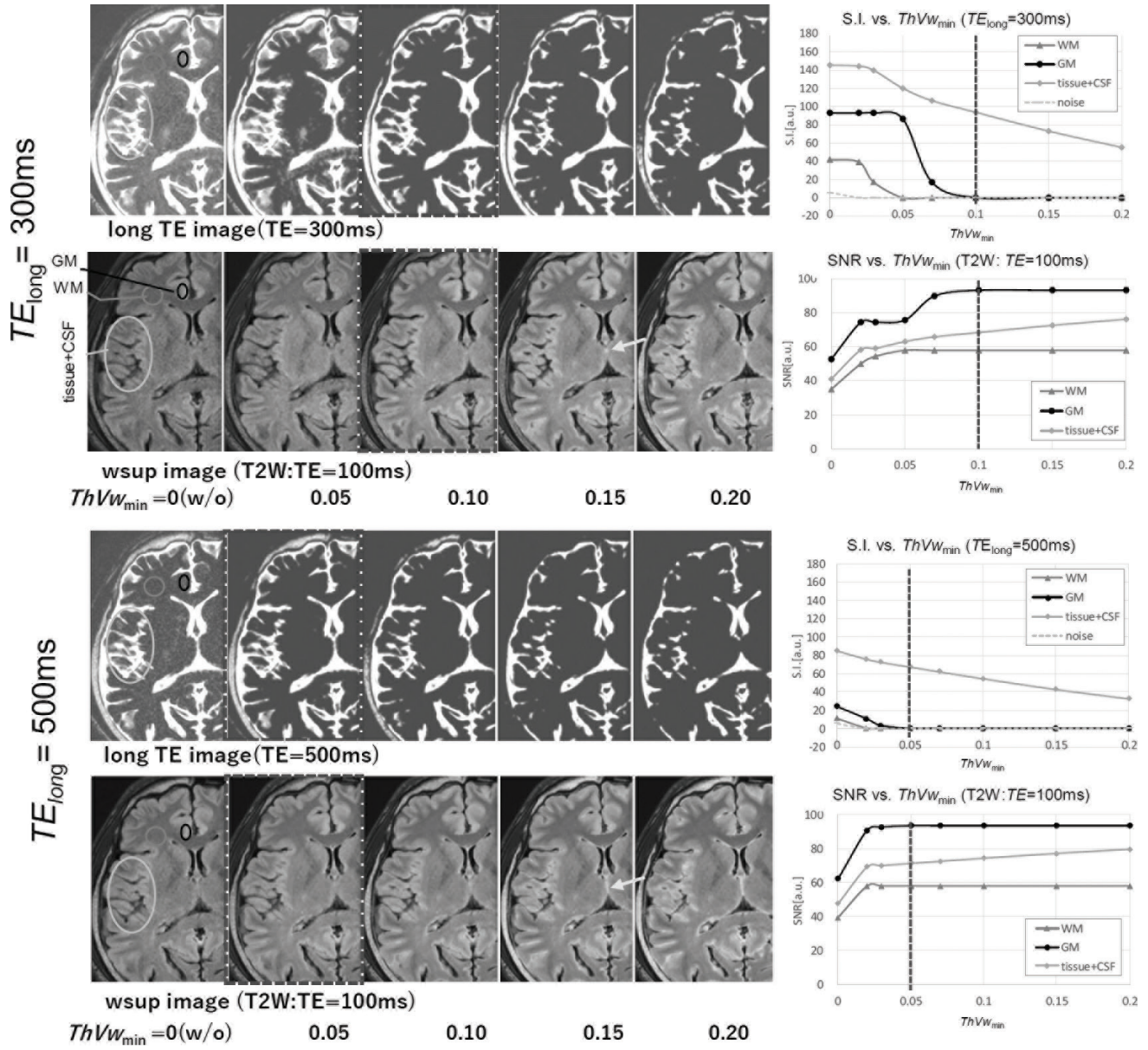

Fig. 6 Results of masking effects as a parameter of ThV_{wmin} for TE_{long} of 300 ms (**a**) and 500 ms (**b**), each shown by 2 images of long TE and T_2WI of TE = 100 ms, signal intensities of long TE images, and SNR of corrected T_2WIs. Although the cerebral spinal fluid (CSF)–partial volume effects (PVE) hyperintensity artifacts remained at Th$V_{wmin} \geq 0.15$ (arrows), those were reduced comparably at $0.05 \leq$ Th$V_{wmin} \leq 0.1$ while the SNRs of GM and WM were improved, compared to those w/o masking (Th$V_{wmin} = 0$). The SNR improvements due to masking were greater for shorter TE_{long}. CSF, cerebral spinal fluid; GM, gray matter; PVE, partial volume effects; T2WIs, T2-weighted images; TE, echo time; WM, white matter.

Parameter optimization

There are several parameters to be determined in our proposed method, such as TE of water dominant image, TE_{long}, thresholding values for making V_w, ThV_{wmax}, and water mask, ThV_{wmin}.

Regarding TE_{long}, it must be selected to be water signal dominant. The tissue signals were almost perfectly reduced below image noises at TE_{long} = 500 ms, but remained at TE_{long} = 300 ms in our healthy volunteer study, as shown in Fig. 6. However, when applied to the long T_2 legions for patients even when using TE_{long} = 500 ms, there is a risk of underestimation of tissue signals after subtraction if the tissue signals remain in long TE images. In such a case, the TE_{long} is set to be even longer, or the greater ThV_{wmin} is used at the price of remaining water signals, as discussed below.

As for the threshold value, ThV_{wmax}, to normalize V_w map, here we used ThV_{wmax} = 1, but it becomes more robust to noises when set to 0.8–0.9 so as to use averaged SI of pure CSF portions. The method for obtaining scaling, $\alpha(TE_m)$ using T_{2w} requires the same TR among all T_2WI of different TEs, and the same value can be used so far as the acquisition

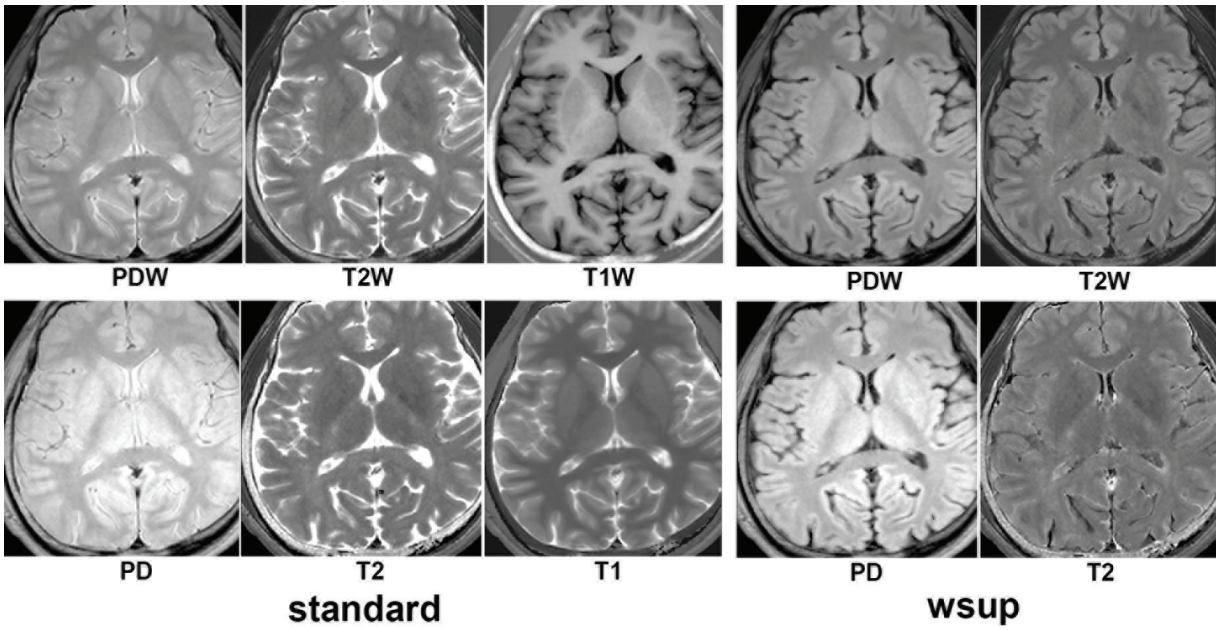

Fig. 7 Acquired images and quantitative maps for standard (left) and wsup (right). The CSF signals in our proposed wsup-images with optimal masking (with ThV_{wmin} = 0.05 using TE_{long} = 500 ms) were suppressed, while the tissue signals were almost comparable with those in the standard. Those numerical results are shown in Table 2. CSF, cerebral spinal fluid; TE, echo time; wsup, water suppression.

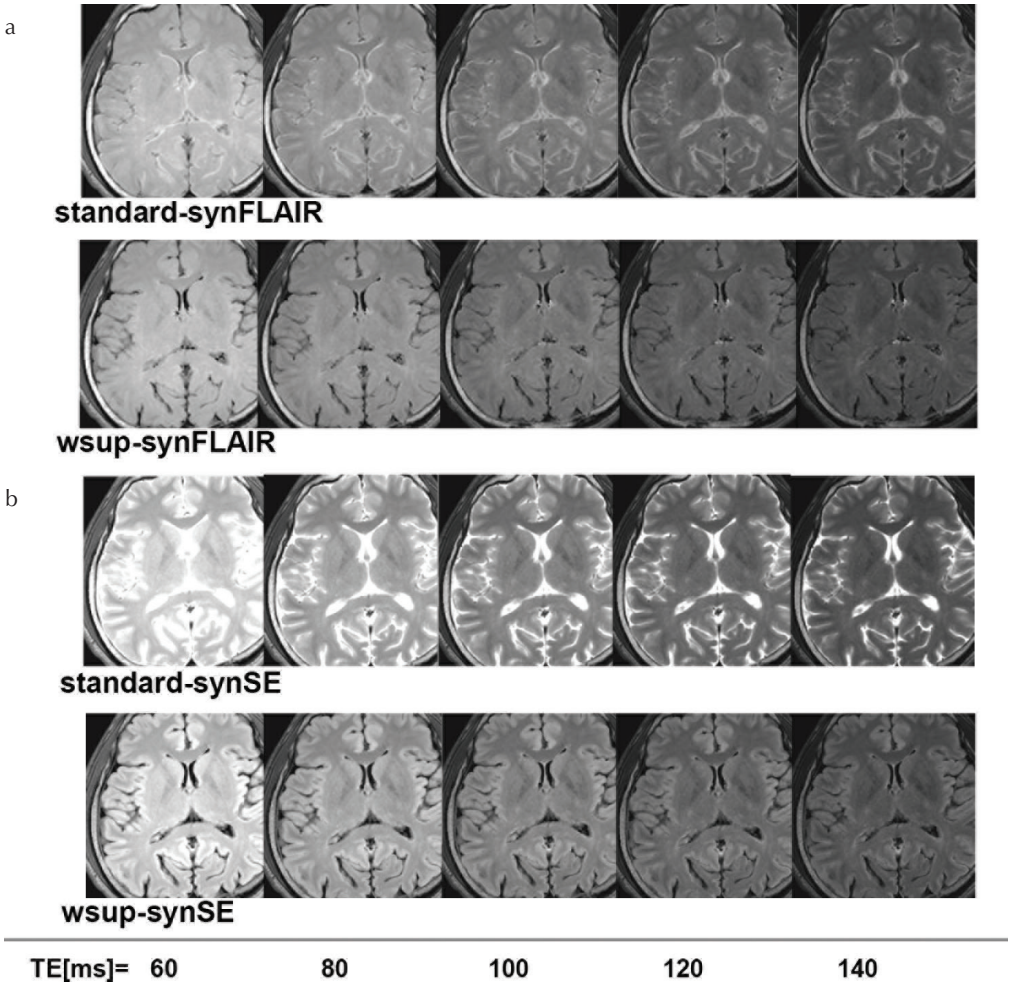

Fig. 8 Synthetic images of FLAIR of (TR, TI) = (10,000 ms, 2700 ms) (**a**) and SE of (TR = 10,000 ms) (**b**) as a parameter of TE for the standard and wsup. The CSF–PVE artifacts in the std-synFLAIR images were reduced dominantly with increasing TE in the wsup-synFLAIR images. In addition, the CSF signals in the std-synSE images were perfectly reduced in the wsup-synSE images. Here, all images are displayed with the same window level and width. CSF, cerebral spinal fluid; FLAIR, fluid-attenuation inversion recovery; PVE, partial volume effect; SE, spin echo; TE, echo time; wsup-syn, water suppression synthetic.

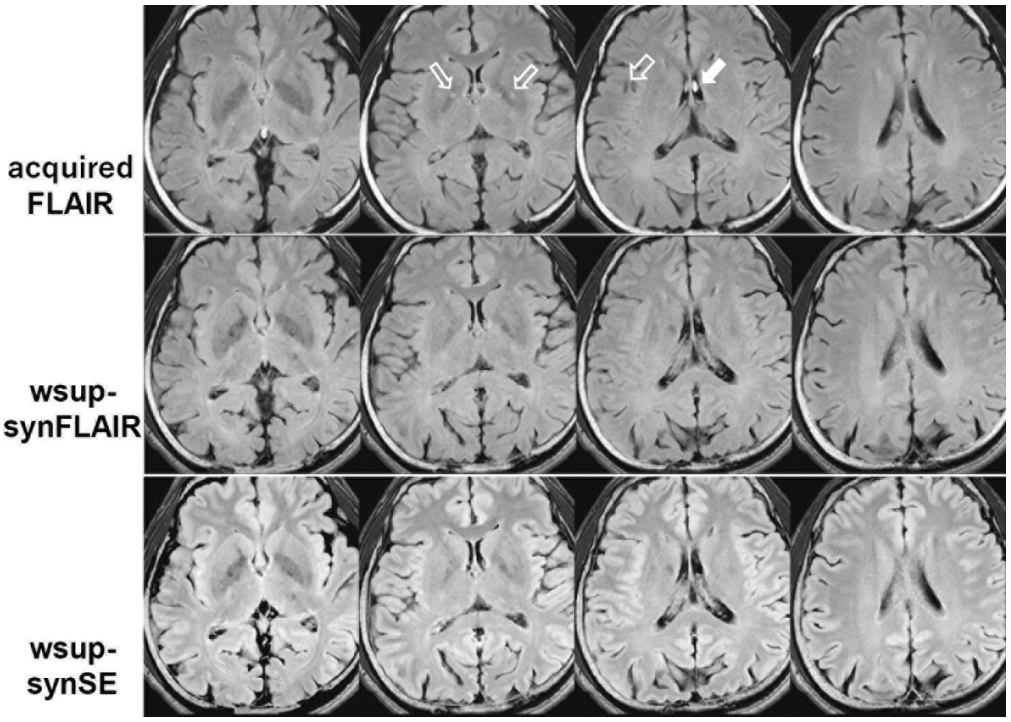

Fig. 9 Comparison of 3 kinds of wsup images of 4 different slices each with acquired FLAIR (top), wsup-syn FLAIR (middle), and wsup-synSE (bottom). Note that the wsup-synFLAIR provided almost equivalent CSF suppression effects and GM–WM contrasts but no artifacts due to CSF inflow (closed arrow) and those motion (open arrows) from the Monro foramen as shown in the acquired FLAIR. In addition, the wsup-synSE provided better GM–WM contrasts than those in the wsup-synFLAIR. Here, TE = 100 ms and the other parameters of FLAIR and SE were same as in Fig. 8, and all images were displayed with the same window level and width. CSF, cerebral spinal fluid; FLAIR, fluid-attenuation inversion recovery; GM, gray matter; SE, spin echo; syn, synthetic; WM, white matter; wsup, water suppression.

Table 2 Numerical volunteer study results of acquired images each with 3 methods of std, wsup w/o, and with masking, where 2 kinds of TE long were used for wsup

Subject		Method	TE_{long} [ms]	SNR				GM–WM CR[a]	GM–WM CNR[a]	noiseSD
				CSF	Temporal (tissue + CSF)	GM	WM			
Acquired SNR, CR, CNR [a.u.]	SE (10000, 20)	std	-	311	221	230	175	0.137	55.6	6.5
		wsup_w/o mask	300	-	132	148	117	0.116	30.8	9.2
			500	-	140	159	122	0.131	36.8	9.2
		wsup_mask	300	-	199	230	175	0.137	55.6	6.5
			500	-	203	230	175	0.137	55.6	6.5
	SE (10000, 100)	std	-	249	87	93	58	0.234	35.3	6.5
		wsup_w/o mask	300	-	42	53	35	0.203	18.1	9.2
			500	-	48	62	39	0.226	23.0	9.2
		wsup_mask	300	-	69	93	58	0.234	35.3	6.5
			500	-	72	93	58	0.234	35.3	6.5
	FLAIR (10000, 2700, 100)	std	-	44	58	67	52	0.128	15.1	6.5

Note that the all data in the wsup w/o masking were restored by the wsup with masking comparably as in the standard data, and the data for TE_{long} of 300 ms were greatly improved by masking subtraction. Analysis parameters were: ThV_{wmax} = 1; ThV_{wmin} = 0.1 (TE_{long} = 300 ms), = 0.05 (TE_{long} = 500 ms). GM–WM CR = $(S_{GM} - S_{WM})/(S_{GM} + S_{WM})$, GM–WM CNR = $(S_{GM} - S_{WM})$/noiseSD, where S_{GM} and S_{WM} are signal intensities of GM and WM. CNR, contrast to noise ratio; CR, contrast ratio; CSF, cerebral spinal flow; GM, gray matter; FLAIR, fluid-attenuation inversion recovery; noiseSD, noise standard deviation; std, standard; TE, echo time; WM, white matter; wsup, water suppression.

condition is fixed. In contrast, the method of using SI ratios of the same water portions with ThV_{wmax} can be applied even among different TR data. A long TR is better for long TE images to measure the PD_w and T_{1w} correctly or to increase the multiple slices in a manner similar to the standard T_2WI, and therefore the latter method is suitable in that case, and the fixed values can also be applied if the acquisition condition is fixed.

In terms of the threshold value, ThV_{wmin} was used to decide water V_w rate for subtraction. With increasing ThV_{wmin}, the area including water signals becomes wider and the longer T_2 tissue signals become easily to be remained, but the risk of SNR reduction becomes smaller. In our experiments with healthy volunteers (Fig. 6), the additional image noises due to subtraction in the wsup image without masking were

Table 3 Numerical volunteer study results of quantitative parameter, and synthetic images, each with 3 methods of std, wsup w/o, and with masking, using the acquired data shown in Table 2

Subject	Method	TE_{long} [ms]	CSF	Temporal (tissue + CSF)	GM	WM	GM–WM CR[a]
Quatitative parameter							
PD [a.u.]	std	-	2238	1829	1878	1497	0.101
	wsup_w/o mask	300	-	1621	1746	1444	0.086
		500	-	1682	1837	1480	0.097
	wsup_mask	300	-	1688	1878	1497	0.101
		500	-	1709	1878	1497	0.101
T_2 [ms]	std	-	987	88	88	72	0.090
	wsup_w/o mask	300	-	70	79	67	0.075
		500	-	76	86	71	0.087
	wsup_mask	300	-	76	88	72	0.090
		500	-	78	88	72	0.090
T_1 [ms]	std	-	3201	1248	1314	819	0.188
Synthetic S.I, CR [a.u.]							
FLAIR (10000, 2700, 100)	std	-	314	424	451	348	0.114
	wsup_w/o mask	300	-	334	392	311	0.104
		500	-	370	434	337	0.112
	wsup_mask	300	-	374	451	348	0.114
		500	-	385	451	348	0.114
SE (10000, 100)	std	-	1696	568	606	376	0.189
	wsup_w/o mask	300	-	386	490	324	0.169
		500	-	443	571	360	0.185
	wsup_mask	300	-	451	606	376	0.189
		500	-	469	606	376	0.189

GM–WM CR = $(S_{GM} - S_{WM})/(S_{GM} + S_{WM})$, where S_{GM} and S_{WM} are signal intensities of GM and WM. CR, contrast ratio; CSF, cerebral spinal flow; GM, gray matter; std, standard; TE, echo time; WM, white matter; wsup, water suppression.

almost perfectly avoided in the wsup image, with the optimal ThV_{wmin} value dependent on the TE_{long}. In addition, if the optimum ThV_{wmin} is set to be greater when the TE_{long} is shorter, the signal of the longer T_2 tissue is reserved without subtraction. The degree of wsup effects and the ratio of remaining tissue signals is a trade-off. Therefore, the ThV_{wmin} needs to be decided experimentally considering the SNR, imaging conditions including TE_{long}, and clinical requirements for the extent of wsup or T_2 values in target tissue or lesion. Once it is decided, the same value can be used in different studies once the TE_{long}, tissue of maximum T_{2t} to be kept, and minimum V_w to be suppressed are decided.

Modification of the proposed method

In our proposed method, the water images of the pure water portions such as ventricles can also be obtained in addition to tissue images. The pure water portions in our wsup quantitative maps become zero or noise. If the correct values are required on pure water portions, the standard quantitative parameter maps should be used. When another parameter to control the ratio of water components, $\alpha_c (0 \le \alpha_c \le 1)$, is applied and it is varied in real time, it will become clinically useful to evaluate the portion of pure or close-to-pure CSF portions. In addition, the long TE image or that quantitative V_w map is also useful for clinical use such as an assessment for glymphatic systems,[9] which have recently gained attention. The V_w map after masking is better than before masking as a quantitative map because it is free of tissue signals or Rician noise.

In addition to the V_w map for the masking to separate tissue and water portions, the standard T_2 map was also studied. However, the V_w map was better than the T_2 map for separating tissue and water portions into small V_w portions. That may be why the sensitivity for separating water from the voxels is higher for the V_w map than for the T_2 map when V_w is small, as shown in our simulation of the standard T_2 versus V_w in Fig. 4. When using the long TE image for the V_w map, high SI noises, the selection of pure CSF portions or the signal inhomogeneity due to B1 must be considered. A combination of T_2 map with long TE image will be useful to make V_w map furthermore robust against those artifacts.

Comparison with alternative approaches

The problem with the original HIRE method[8] was the SNR reduction in longer T_2 lesions due to a simple subtraction of the long TE image of the relatively shorter TE of 240 ms as water-dominant TE. To solve this, a modified method was proposed,[10] where a non-linear conversion of the long TE image was performed before subtraction to suppress the lower SI. However, that method is not suitable for quantitative mapping because the degree of wsup varies depending on the TE or spatial position. In contrast, in our proposed method, as shown in Table 2, the tissue T_2 is not varied after our wsup with masking because the same scaling of 0 or 1 by spatial masking then-suitable TE-dependent scalings to correct SIs of long TE images is performed before subtraction.

Other alternative approaches to reduce the CSF–PVE artifacts in synMRI are a 3D acquisition[11,12] or a combination with deep learning (DL) technique to use acquired FLAIR image as a teacher.[13,14] However, the PVE artifacts cannot be principally avoided even when using small voxels, and DL is a complicated procedure and the robustness of suppression is unclear. In contrast, our proposed technique is very simple and easily combined with the conventional synthetic MRI technique.

More generally, unknown parameters for such a bi-exponential model can be principally obtained by applying a least-square algorithm to the different TE data of multiple points more than the number of unknown parameters; however, this is usually ill-posed problem and difficult to obtain a stable solution under noise contamination. Bayesian approaches[15,16] have succeeded in improving the robustness of stabilities to noises for bi-exponential decay data based on a two-compartment model. In this case, two parameters of (V_w, T_{2t}) can be calculated with fixing T_{2w} in Eq. (3) or Eq. (4) if the number of data points is over 3. Here we used the minimum number of different TE images ($M = 3$ including long TE) to obtain wsup maps of tissue. However, those approaches require many data points and longer processing time due to the use of a non-linear solution. Better separation is not expected unless longer TE_{long} or some thresholding technique is used to improve the accuracy of separating components of longer T_2 tissue and water even when using multiple data points.

More recently, a novel method called "MR fingerprinting (MRF)," which enables quantitative maps of T_1, T_2, and PD to be obtained very fast, was proposed,[17,18] and it is beginning to be applied widely. The MRF uses data obtained by steady-state free precession (FISP) sequence with varying TR, flip-angle (FA), and *k*-space under-sampling, then matches the data with the dictionary-described relationship between the data and parameters based on the Bloch equation. In addition, a machine-learning approach using DL combined with the MRF technique was proposed[19] and solved the shortcomings of dictionary size and computing load in current MRF techniques. It is generally difficult for the FISP to obtain pure water images compared with the FSE we used. However, in the future, those approaches might solve the multi-parameter model problem,[20] which is the difficulty of current non-linear fitting by combination with the acquisition technique to reflect a wider range of quantitative parameters, including tissue to water components, while keeping quantization resolution.

Conclusion

Our proposed T_2wsup-synMRI technique makes it easy to reduce the CSF–PVE artifacts problematic in the synthetic FLAIR images using the current synMRI technique by adding long TE images and simple processing. Although further optimizations in data acquisition and processing techniques are required before actual clinical use, we expect our technique to become clinically useful.

Acknowledgments

We express our sincere thanks to Yuki Takai and Ryo Shiroishi, and Hitoshi Kanazawa in Canon Medical Systems Corporation for supporting data acquisition and analysis in this study. Our preliminary report was shown in Kimura et al.[21,22]

Conflicts of Interest

We have no conflicts of interest to declare.

References

1. Warntjes JB, Leinhard OD, West J, Lundberg P. Rapid magnetic resonance quantification on the brain: optimization for clinical usage. Magn Reson Med 2008; 60:320–329.
2. Tanenbaum LN, Tsiouris AJ, Johnson AN, et al. Synthetic MRI for clinical neuroimaging: results of the Magnetic Resonance Image Compilation (MAGiC) prospective, multicenter, multireader trial. AJNR Am J Neuroradiol 2017; 38: 1103–1110.
3. Hagiwara A, Warntjes M, Hori M, et al. SyMRI of the brain: rapid quantification of relaxation rates and proton density, with synthetic MRI, automatic brain segmentation, and myelin measurement. Invest Radiol 2017; 52:647–657.
4. Hagiwara A, Hori M, Yokoyama K, et al. Synthetic MRI in the detection of multiple sclerosis plaques. AJNR Am J Neuroradiol 2017; 38:257–263.
5. Granberg T, Uppman M, Hashim F, et al. Clinical feasibility of synthetic MRI in multiple sclerosis: a diagnostic and volumetric validation study. AJNR Am J Neuroradiol 2016; 37:1023–1029.
6. Hagiwara A, Hori M, Yokoyama K, et al. Utility of a multiparametric quantitative MRI model that assesses myelin and edema for evaluating plaques, periplaque white matter, and normal-appearing white matter in patients with multiple sclerosis: a feasibility study. AJNR Am J Neuroradiol 2017; 38:237–242.
7. Andica C, Hagiwara A, Nakazawa M, et al. Synthetic MR imaging in the diagnosis of bacterial meningitis. Magn Reson Med Sci 2017; 16:91–92.
8. Essig M, Deimling M, Hawighorst H, Debus J, van Kaick G. Assessment of cerebral gliomas by a new dark fluid sequence,

high intensity REduction (HIRE): a preliminary study. J Magn Reson Imaging 2000; 11:506–517.
9. Louveau A, Smirnov I, Keyes TJ, et al. Structural and functional features of central nervous system lymphatic vessels. Nature 2015; 523:337–341.
10. Deimling M. Magnetic resonance tomography apparatus and method for operating same for image generation. US patent 7,340,290 B2, 2002.
11. Hwang KP, Banerjee S, Zhang T, Warntjes M. 3D isotropic multi-parameter mapping and synthetic imaging of the brain with 3D-QALAS: comparison with 2D MAGIC. Proceedings of 26th Annual Meeting of SMRM, Paris, France, 2018; 5627.
12. Kvernby S, Warntjes M, Engvall J, Carlhäll CJ, Ebbers T. Clinical feasibility of 3D-QALAS - Single breath-hold 3D myocardial T1- and T2-mapping. Magn Reson Imaging 2017; 38:13–20.
13. Gong E, Banerjee S, Pauly J, Zaharchuk G. Improved synthetic MRI from multi-echo MRI using deep learning. Proceedings of 26th Annual Meeting of ISMRM, Paris, France, 2018; 2795.
14. Hagiwara A, Otsuka Y, Hori M, et al. Improving the quality of synthetic FLAIR images with deep learning using a conditional generative adversarial network for pixel-by-pixel image translation. AJNR Am J Neuroradiol 2019; 40:224–230.
15. Larry Bretthorst G, Hutton WC, Garbow JR, Ackerman JJH. Exponential parameter estimation (in NMR) using Bayesian probability theory. Concept Magn Reson A 2005; 27A: 55–63.
16. Bouhrara M, Reiter DA, Spencer RG. Bayesian analysis of transverse signal decay with application to human brain. Magn Reson Med 2015; 74:785–802.
17. Ma D, Gulani V, Seiberlich N, et al. Magnetic resonance fingerprinting. Nature 2013; 495:187–192.
18. Badve C, Yu A, Rogers M, et al. Simultaneous T_1 and T_2 brain relaxometry in asymptomatic volunteers using magnetic resonance fingerprinting. Tomography 2015; 1:136–144.
19. Golbabaee M, Chen D, Gómez PA, et al. Geometry of deep learning for magnetic resonance fingerprinting. International Conference on Acoustics, Speech, and Signal Processing (ICASSP), Brighton, United Kingdom, 2018.
20. Vidyullatha P, Rajeswara Rao D. Machine learning techniques on multidimensional curve fitting data based on r- square and chi-square methods. Int J Electr Comput Eng 2016; 6:974–979.
21. Kimura T, Takai Y, Kusahara H, et al. Synthetic MRI with water suppression technique to reduce CSF partial-volume artifacts. Proceedings of 27th Annual Meeting of ISMRM, Montreal, Canada, 2019; 4867.
22. Kimura T, Yamashita K, Fukatsu K. Synthetic-MRI with T2-based water suppression without loss of tissue SNR. Proceedings of the 29th Annual Meeting of ISMRM, Paris, France, 2020; 3775.